Elaboration and evaluation of alginate foam scaffolds for soft tissue engineering

Ceccaldi Caroline[a,b,1], Bushkalova Raya[a,b,1], Cussac Daniel[b,c], Duployer Benjamin[f], Tenailleau Christophe[f], Bourin Philippe[e], Parini Angelo[b,c,d], Sallerin Brigitte[b,c,d,2], Girod Fullana Sophie[a,*,2]

[a] CIRIMAT, Université de Toulouse, CNRS, INPT, Université Toulouse 3 Paul Sabatier, Faculté de Pharmacie, F-31062 Toulouse, France
[b] INSERM, UMR 1048, F-31432 Toulouse, France
[c] Université de Toulouse, UPS, Faculté des Sciences Pharmaceutiques, F-31062 Toulouse, France
[d] CHU Toulouse, Pôle Pharmacie, F-31432 Toulouse, France
[e] EFS, Laboratoire de thérapie cellulaire, F-31027 Toulouse, France
[f] Université de Toulouse, CIRIMAT, UPS-INPT-CNRS, F-31062 Toulouse, France

Keywords:
Alginate
Foam-based scaffolds
Surfactants
Mesenchymal stem cells
Soft tissue engineering

A B S T R A C T

Controlling microarchitecture in polymer scaffolds is a priority in material design for soft tissue applications. This paper reports for the first time the elaboration of alginate foam-based scaffolds for mesenchymal stem cell (MSC) delivery and a comparative study of various surfactants on the final device performance. The use of surfactants permitted to obtain highly interconnected porous scaffolds with tunable pore size on surface and in cross-section. Their mechanical properties in compression appeared to be adapted to soft tissue engineering. Scaffold structures could sustain MSC proliferation over 14 days. Paracrine activity of scaffold-seeded MSCs varied with the scaffold structure and growth factors release was globally improved in comparison with control alginate scaffolds. Our results provide evidence that exploiting different surfactant types for alginate foam preparation could be an original method to obtain biocompatible scaffolds with tunable architecture for soft tissue engineering.

1. Introduction

For the past decades, there has been a growing interest in the use of Mesenchymal Stem Cells (MSCs) to regenerate biological tissues after several acute and chronic diseases. After an initial focus on their capacity to differentiate into mesodermal lineage, they are now acknowledged for their positive effects attributed to their paracrine activities, which allow direct regeneration as well as indirect modulatory effects on damaged and diseased tissues. MSCs secrete paracrine factors which promote tissue repair, stimulate proliferation and differentiation of endogenous tissue progenitors, and decrease inflammatory/immune reactions (Caplan, 2007; Li and Ikehara, 2013; Souidi et al., 2013). Such therapeutic properties are particularly effective in ischemic diseases treatment of the heart (Léobon et al., 2009; Panfilov et al., 2013), kidneys (Alfarano et al., 2012; Furuichi et al., 2012) and lungs (Chen et al., 2012; Yip et al., 2013). In these treatments, MSCs are delivered to the targeted organ by injection into the perfusing artery or directly into the tissue surrounding the damaged area. Unfortunately, benefits of such therapeutic approaches are limited by poor cell retention and early cell death at the injury site after implantation. Indeed, several studies have reported that more than 80–90% of transplanted cells die within the first 72 h after injection (Maurel et al., 2005; Toma et al., 2002). Multiple mechanisms are involved in these early cell losses including hypoxia, local inflammation and mechanical stress occurring during cell administration. Improvement of cell concentration and viability at the injury site, in order to promote their therapeutic activity, is becoming a priority in the field of cell therapy.

One promising strategy is to associate MSCs with a biocompatible material that protects and concentrates them on the damaged area. The ideal scaffold should improve viability of grafted MSCs, preserve their paracrine activity and provide an artificial matrix

* Corresponding author at: CIRIMAT, Université de Toulouse, CNRS, INPT, UPS, Université Toulouse 3 Paul Sabatier, Faculté de Pharmacie de Toulouse, 35 chemin des Maraichers, 31062 Toulouse cedex 9, France.
E-mail address: sophie.fullana-girod@univ-tlse3.fr (G.F. Sophie).
[1] These authors provided equal contribution to this work (first author).
[2] These authors provided equal contribution to this work (last author).

allowing medium/long term cell survival as well as their secretion function. In addition, the mechanical properties of the selected material must not only be compatible with soft tissues but also appropriate for surgery manipulations during implantation on the damaged tissue. Scaffold architecture is another critical parameter that could affect the biological activity of entrapped cells and the fate of the implanted device. More specifically, it has been reported that pore size distribution and pore interconnectivity affect cell morphogenesis (Zmora et al., 2002), stem cell behavior and implant's colonization by host cells (Salem et al., 2002; Souidi et al, 2013; Toma et al., 2002; Zeltinger et al., 2001).

Among materials used for cell therapy, natural polymers seem to be particularly adapted in terms of biocompatibility (Lee and Mooney, 2001). In that regard, alginates are among the most widely used polymers (Andersen et al., 2015; Bidarra et al., 2014; Giovagnoli et al., 2015; Ruvinov and Cohen, 2016; Silva et al., 2015) due to their low toxicity after purification, gelling properties (under conditions compatible with biological activities: 37 °C, pH 7.4 . . .), structural resemblance to the extracellular matrix (considered to be at the origin of their excellent biocompatibility), and relatively low cost. Regarding their origin and chemical structure, alginates are naturally occurring anionic linear (unbranched) polysaccharides, which can be extracted from kelp, brown seaweed and some bacteria. They are salts of alginic acid consisting of 1,4-linked β-D-mannuronic (M) and α-L-guluronic (G) residues organized in regions of sequential G units (G-blocks), regions of sequential M units (M-blocks) and regions of G and M units atactically organized. Their sol–gel transition properties are based on the formation of a stiff "egg-box" structure due to divalent cations selective binding to the G-blocks of two adjacent polymeric chains (Grant et al., 1973). The major issue limiting the widespread use of alginate hydrogels as tissue engineering scaffolds is the possible exchange of divalent cations with monovalent cations over time (Bajpai and Sharma, 2004), resulting in crosslinks dissociations in the gel's network followed by a mechanical degradation. However, alginates' mechanical behavior is easily modifiable by different crosslinking or by changing the type and/or the molecular weight distribution to match the required stiffness of host tissues (Augst et al., 2006). Moreover, the degradation rate depends not only on alginates' characteristics, but also on the device's dimensions and implantation site. For example, alginate microspheres injected under the renal capsule were almost intact 4 weeks after implantation (Trouche et al., 2010); it was also the case for G-type alginate scaffolds implanted on rat myocardium but not for M-type alginate scaffolds (Ceccaldi et al., 2012). Thus, an accurate choice of alginate type/properties could allow a wide range of biomedical applications.

The biocompatibility of alginates has been extensively described in the literature and for the last few decades, the scientific community has worked to established efficient methods to produce alginates with high purification grades and limited amount of polyphenols, endotoxins and protein residues which can impact the inflammatory reaction after implantation (Klock et al., 1997; Leinfelder et al., 2003; Tam et al., 2006). In general, alginates are not known to be biologically active. In fact, protein adsorption and cell attachment are low due to their high water content, dense negative surface charge, and the lack of molecular recognition by cell surface receptors (Dvir-Ginzberg et al., 2008; Gandhi et al., 2013; Glicklis et al., 2000). This particularity of alginates, combined with their strictly local effect (on the application site), have allowed the material to be qualified as safe for human application. Furthermore, several clinical trials using alginate-based medical devices are currently in progress (AUGMENT-HF: NCT01311791; PRESERVATION 1: NCT01226563; NCT01734733; NCT00521937) or completed (GLP-1 CellBeads®: NCT01298830; DIABECELL®: NCT00940173; NCT01396304), demonstrating the growing interest in the use of this polymer for biomedical applications.

Regarding tissue engineering applications, macroporous three-dimensional (3D) alginate scaffolds are of particular interest. Indeed, compared to non-macroporous hydrogels they provide to cells a biomimetic environment, allow improved cell infiltration, better diffusion of solutes, nutrients and oxygen, as well as enhanced waste removal (Shapiro and Cohen, 1997). Additionally, despite the non-adhesive nature of alginate polymers, cells are efficiently incorporated and retained within 3D alginate sponges due to the porous structure of the matrix whereas they are not on bi-dimensional (2D) alginate films (Dvir-Ginzberg et al., 2008; Glicklis et al., 2000). A number of studies have shown benefits when using alginate macroporous scaffolds for 3D cell culture (Sapir et al., 2011; Caplan, 2007; Li and Ikehara, 2013; Shachar and Cohen, 2003; Shapiro and Cohen, 1997; Zieber et al., 2014) and for soft tissues regeneration (Dvir et al., 2009; Dvir-Ginzberg et al., 2008; Leor et al., 2000). In particular, foaming alginates has allowed obtaining highly porous scaffolds with tunable morphology and mechanical characteristics according to the type and concentration of alginate used as well as the source of gelling ions (Andersen et al., 2012, 2014a). In addition, alginate foams appeared to be highly compatible for cell entrapment, prolonged 3D cell culture and retrieval of NHIK 3025 and NIH: 3T3 cells (Andersen et al., 2014b). In our study, we wished to produce foam-based alginate porous scaffolds specifically adapted for MSC use in cell therapy, *i.e.* tailored for MSC immobilization and improvement of their secretion ability. For alginate foaming, we have chosen to use surfactants coming from the polysorbates (Montanox®) and the poloxamers (Pluronic®) families, as they are non-ionic, water soluble (hydrophilic–lipophilic balance >8), biocompatible, and certified for biomedical applications (Andersen et al., 2012; Bueno et al., 2014; Eiselt et al., 2000; Fowler et al., 2002; Inzana et al., 2014; Tadros, 2005; Vashi et al., 2008). More precisely, we used four of these surfactants as we had observed them to be compatible with MSC culture (based on a preliminary evaluation of their cytotoxicity and water solubility): Montanox 20, Montanox 80, Pluronic 127 and Pluronic 108. Mixing each one of them with an alginate solution followed by a freeze-drying, permitted the generation of four different foam-based scaffolds. They were characterized with regard to their architecture, porosity, mechanical properties and cell-seeding ability with functional MSCs. Finally, cell viability as well as cell secretion function were also investigated in order to ascertain the most promising formulations for soft tissue cell therapy.

2. Materials and methods

Ultrapure MVG sodium alginate with a M/G ratio of 0.47 (determined by ^{1}H NMR measurement) was purchased from Provona Biopolymer Inc. (Novamatrix, Norway). Sodium bicarbonate was furnished by Cooper (France). Montanox and Pluronic surfactants were provided by Seppic (France) and BASF Corporation (France), respectively. HEPES (4-(2-hydroxyethyl)-1-piperazineethanesulfonic acid) sodium salt was purchased form Sigma–Aldrich, France. Sodium chloride (NaCl) and calcium chloride dehydrate ($CaCl_2{\cdot}2H_2O$) were purchased from VWR. Reagents used for *in vitro* cell culture were α-Minimum Essential Medium (α-MEM, Invitrogen, San Diego, CA, USA) supplemented with 10% fetal calf serum (Hyclone, Logan, UT, USA) and ciprofloxacin (10 mg ml^{-1}; Bayer Schering Pharma, Germany).

2.1. Macroporous scaffolds elaboration

Solutions of 3% (w/w) MVG alginate were prepared in iso-osmotic saline solution during 30 min at 1800–2000 rpm

(Heidolph RZR-2041, Germany). 0.9% (w/w) sodium bicarbonate and 1% (w/w) surfactant (Montanox 80, Montanox 20, Pluronic F127 or Pluronic F108) were added and stirred during 30 min to incorporate air bubbles until a stable foam was obtained.

Three-dimensional scaffolds were generated by a freeze-drying technique. Briefly, aliquots (500 μl) of the polymer solutions were placed in a 48-well plate, frozen overnight at −20 °C, and lyophilized. The constructs were then cross-linked in an iso-osmotic buffer containing calcium ions (150 mM NaCl, 0.1 M $CaCl_2 \cdot 2H_2O$, 10% w/w acetic acid) during 30 min. The obtained scaffolds were washed 3 times (10 min each) in a HEPES buffer and lyophilized again. All studied scaffolds were prepared under aseptic conditions and finally exposed to UV light. The final scaffolds dimensions, used in all experiments, were 10 mm diameter × 5 mm thickness.

2.2. Foam stability evaluation

Foam stability was evaluated by measuring the foam volume in a graduated test tube at determined time intervals. Results are expressed as a percentage of the final foam volume measured 24 h after preparation.

2.3. Scanning electron microscopy (SEM)

SEM analyses of surfaces and cross-sections of dried 3D scaffolds were performed with a Leo 435 VP scanning electron microscope. Samples were mounted on an aluminum sample mount and sputter-coated with silver. The specimens were observed at a 10 kV accelerating voltage.

2.4. Computed X-ray micro-tomography (micro-CT)

The micro-CT study of samples was carried out on Phoenix Nanotom 180 (GE Sensing, Germany) using the following parameters: 30 kV voltage, 160 μA current, no filter material, 0.25° rotation step, 5 frames as frame averaging, 1440 tomographic projections over a 360° scan angle, 1 s exposure time. A binning 2 × 2 was applied for the slices reconstruction and the resulting voxel size was 11.5 μm^3. 3D virtual models of scaffolds were obtained using VGStudio MAX 2.1. A region of interest (ROI) was drawn within the reconstructed volume and a threshold was defined to identify the polymeric phase. Then, a morphometric analysis of the ROI was performed to obtain the total porosity and voids interconnectivity. Scaffolds' morphologies were analyzed on the basis of 2D X-ray tomographic slicesusing ImageJ (NIH, USA). Calculations were done on a ROI defined on the surface and in the cross-section of each scaffold. Feret's diameters were obtained and pore densities were calculated as the total void number/ROI area (**n = 10 slices per scaffold**). Voids on edges were excluded.

2.5. Evaluation of scaffolds stability upon rehydration

Scaffolds swelling behavior was evaluated by weighing them every 10 min after immersion in cell culture medium. The swelling ratio was calculated according to the following formula:

$$\text{Swelling ratio} = \frac{(W_t - W_0)}{W_0}$$

where W_t is the scaffold weight at time t and W_0 is the weight of the dried scaffold before placing it in culture medium.

2.6. Fourier transform infrared spectroscopy (FTIR)

Dried samples were mixed with KBr (Fluka, France) and pressed into a pellet. FITR spectra were recorded between 400 and 4000 cm^{-1} using Spectrum One FT-IR Spectrometer (Perkin Elmer, France).

2.7. Mechanical properties evaluation

Differential elastic moduli and mechanical behavior of the scaffolds were followed by three successive uniaxial compressive assays (TA-XT2 Texture Analyzer, Stable Microsystems, UK). The apparatus consisted of a mobile probe (314.16 mm^2) moving vertically up and down at a constant and predefined velocity (0.5 mm s^{-1}). The force exerted by the probe on the scaffolds was recorded as a function of the displacement. Then, the force was converted into stress by reporting the force to the surface of force application and the displacement was converted to a strain percentage in comparison with the initial dimension. Differential elastic moduli were calculated from the stress–strain curves at 50% of strain and represent the relative stiffness of the scaffold at 50% strain. The differential elastic modulus was expressed as follows from at least three independent observations: $E_{50\%} = [(F_{50\%}/S)/\text{Strain}] \times 1000$ kPa, where $F_{50\%}$ is the force registered at 50% strain (N) and S is the surface of the specimen (mm^2).

2.8. Isolation and culture of human MSCs *for* in vitro *experiments*

Human MSCs were isolated from PBS-washed filters used during bone marrow graft processing for allogenic bone marrow transplantation. Cells were cultured at a density of 5×10^4 cells cm^{-2} in α-Minimum Essential Medium supplemented with 10% fetal calf serum and ciprofloxacin (10 mg ml^{-1}). After 72 h at 37 °C in 5% CO_2, non-adherent cells were removed and the medium was changed. Cultures were fed every 3–4 days. MSCs were used between the 3rd and the 6th passage.

2.9. MSC seeding and cultivation

For *in vitro* studies, cells were seeded within the scaffolds by centrifugation (400 g, 1 min) after dropping 15 μl of cell suspension containing 20,000 cells on the top of the dried scaffolds ($n = 3$ for each experimental condition). The cell-seeded scaffolds were hydrated by adding 985 μl of culture medium to each scaffold. The constructs were cultured at 37 °C in 5% CO_2 and the medium was changed every 3–4 days.

2.10. LIVE/DEAD assay and confocal microscopy

LIVE/DEAD assays were performed using the Viability/Cytotoxicity kit (FluoProbes®, Interchim, France). Briefly, 4 h after seeding, constructs were washed two times with α-MEM/physiological serum (1/1) and immersed (30 min, 37 °C) in the presence of 2 μM ethidium homodimer-3 (necrotic marker measuring nucleus membrane integrity) and 1 μM calcein AM (viability marker measuring the intracellular esterase activity) to stain dead cells in red and live cells in green. After a washing with physiological serum, scaffolds were observed under a confocal microscope (Zeiss LSM 510) using a ×10 objective. Samples were excited with a 488 nm Argon laser and with a 543 nm helium–neon laser. The emitted fluorescence was collected using two separate photo multiplier tubes with a BP 500–560 nm filter for calcein detection and a LP 620 nm filter for ethidium homodimer-3 detection.

2.11. Quantification of MSC metabolism activity

Cell metabolism activity was quantified by AlamarBlue® assay (Molecular Probes, Invitrogen, France). 3D scaffolds were transferred to new wells and incubated with 1 ml of α-MEM supplemented with 10% of AlamarBlue® reagent for 1–4 h as specified by the manufacturer. Aliquots of 100 µl were transferred to a 96-well plate and the fluorescence was measured at an excitation wavelength of 540 nm and an emission wavelength of 620 nm using a plate reader (Infinite®200Pro, Tecan Group).

2.12. Growth factors release quantification

After cell seeding, scaffolds were hydrated by adjusting the volume of culture medium and cultured at 37 °C in 5% CO_2 for 24 h under sterile conditions. The amount of HGF, FGF-2 and VEGF released into the medium was quantified in the supernatant by xMAP technology (Luminex 100™ system, Luminex Corp.) with anti-human HGF, FGF-2 and VEGF antibodies (Ozyme, France).

2.13. Statistical analysis

Results are expressed as mean ± SEM. Statistical comparison of the data was performed using one-way ANOVA and *post hoc* Bonferroni's test for comparison of more than two groups. For the mechanical tests, a two-way ANOVA was used to analyze changes over time among the experimental groups. A value of $P < 0.05$ was considered significant.

3. Results

3.1. Stability of alginate foams prepared using various surfactants

Alginate foams were produced by mixing 3% (w/w) alginate solution with bicarbonate and 4 various surfactants as foam stabilizers: Montanox 80, Montanox 20, Pluronic F127 or Pluronic F108. The foams stability was studied after 30 min of mixing at 1800–2000 rpm and Fig. 1 shows the stability of the foam over time during 6 h. Foams were stable for all formulations tested, showing that the 4 surfactants selected for this study are adapted to prepare foam-based scaffolds after gelation and drying steps.

3.2. Morphology and porosity of alginate foam-based scaffolds

Four different scaffolds with a constant alginate concentration (3% w/w) were prepared in the presence of Montanox 80, Montanox 20, Pluronic F127 or Pluronic F108 surfactants, as described in Section 2. Control scaffolds composed by pure alginate (without surfactants) were also prepared, according to the same procedure. Fig. 2 shows SEM images of the surface and the cross-section of control alginate scaffolds (REF-S, Fig. 2A and F), and of alginate scaffolds obtained in the presence of Montanox 80 (Mx80-S: Fig. 2B and G), Montanox 20 (Mx20-S: Fig. 2C and H), Pluronic F127 (F127-S: Fig. 2D and I) and Pluronic F108 (F108-S: Fig. 2E and J).

SEM micrographs presented in Fig. 2 reveal a highly porous and interconnected morphology both on surface and in cross-section of all freeze-dried scaffolds. Quantitative data obtained by micro-CT shows that the mean pore size ranged from 100 to 200 µm on surface, and from 100 to 230 µm in cross-section, depending on the surfactant used in the preparation step. The highest pore density was obtained using Pluronic 108 and the lowest pore density was obtained using Montanox 20 and Pluronic 127, both on surface and in cross-section (Fig. 2K and L). The total porosity spanned from 80% to 98% (Table 1) and the voids interconnectivity was 100% for all scaffolds, meaning that all pores were connected to the surface (data not shown). It is interesting to notice the variety of 3D porous architectures of the scaffolds generated by using two different families of surfactants (Montanox and Pluronic) compared to each other and to the reference scaffold without surfactant (Fig. 3A and B).

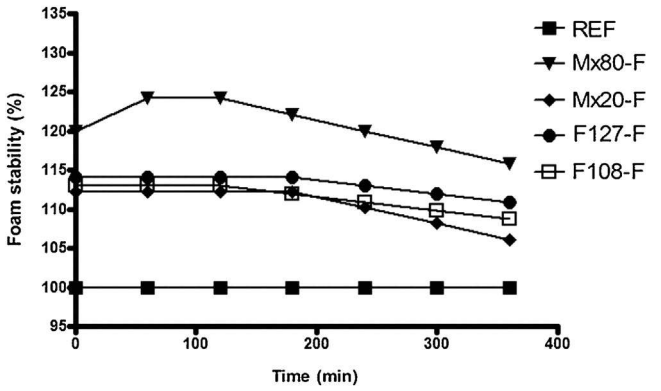

Fig. 1. Foam stability over time of alginate foam solutions (Mx80-F, Mx20-F, F127-F and F108-F) prepared using different stabilizing agents (Montanox 80, Montanox 20, Pluronic F127 and Pluronic F108) or without a stabilizing agent (REF).

3.3. Presence of surfactant residues within 3D scaffolds

Surfactants are amphiphilic molecules and are therefore able of inserting into the plasma membrane of the entrapped cells. Consequently, it is indispensable to wash the scaffolds after preparation in order to eliminate all surfactant residues. Scaffolds were washed 3 times in HEPES buffer bath and residues of surfactant were tracked by FITR. To that end, we first determined wavenumbers of specific infrared peaks of each surfactant and then checked their absence in the final scaffolds spectra. Their characteristic peaks were situated at 2859 cm^{-1} and 1105 cm^{-1} for Montanox 80; 2869 cm^{-1}, 1732 cm^{-1}, 1460 cm^{-1}, 1346 cm^{-1} and 1100 cm^{-1} for Montanox 20; 2884 cm^{-1}, 1467 cm^{-1}, 1341 cm^{-1} and 1240 cm^{-1} for Pluronic F127 and F108 (Fig. 4A). Concerning the final scaffolds spectra (Fig. 4B), they presented the characteristic peaks of alginate at 1033 cm^{-1} and 1091 cm^{-1}, corresponding to the glucuronic (G) and the mannuronic (M) acid units, respectively. The —OH stretching peak was observed at 3407 cm^{-1}. The H—C—H and O—C—H stretching vibration was seen at 1421 cm^{-1}. The $—COO^-$ stretch was visible at 1609 cm^{-1}. The peaks at 881 cm^{-1} and 816 cm^{-1} indicated β-glycosidic linkages between G and M units of alginates. Thus, the FTIR analysis allowed us to demonstrate that alginate scaffolds spectra were not contaminated by the surfactant specific peaks after the three washing steps in a HEPES buffer.

3.4. Scaffolds' behaviors upon hydration

Swelling behavior was followed during rehydration in α-MEM. It was determined every 10 min for each scaffold during 150 min. Fig. 5 shows that swelling rates were higher (around 20–40 times) after 2 h of immersion in cell culture medium and remained stable over time for all scaffold types (Panel A). No scaffold degradation was observed during the experiments. Panel B shows that alginate scaffolds preserve their morphology after rehydration. These results suggest that the scaffold integrity was preserved during the rehydration in cell culture medium and, therefore, that scaffolds could support 3D cell culture.

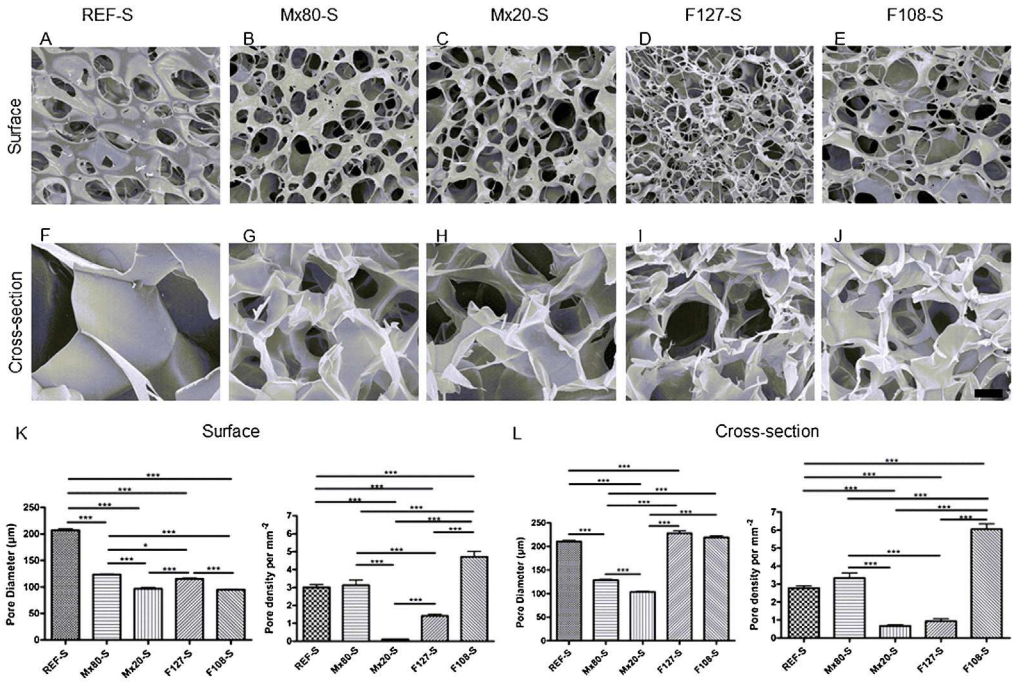

Fig. 2. Morphology and porosity of macroporous scaffolds obtained with various stabilizing agents. Representative SEM images of scaffolds surfaces (Panel A to E) and cross-sections (Panel F to J). Scale bar corresponds to 50 µm (magnification at 250×). Determination of surface (Panel K) and cross-section (Panel L) porosity and pore density of macroporous scaffolds (measures made on 2D micro-CT images). *: $p \leq 0.05$ and ***: $p \leq 0.001$, based on Anova analysis.

Table 1
Porosity of the different alginate scaffolds, as determined by micro-CT analysis. The total porosity (void volume/total volume of the ROI) is calculated from a 2D ROI drawn within the reconstructed volume of the entire scaffold.

Samples	Porosity (%)
REF-S	85.12
Mx80-S	80.06
Mx20-S	97.96
F108-S	91.98
F127-S	88.29

3.5. Mechanical properties of 3D scaffolds under compression

Mechanical behaviors of rehydrated scaffolds were assessed by 3 successive compressions and their elastic moduli were determined at 50% of strain (Fig. 6). The matrices prepared in the presence of surfactants presented lower mechanical properties in the first compression cycle (Mx80-S: 11 ± 2.5 kPa; Mx20-S: 22.2 ± 1 kPa; F127-S: 10.53 ± 2.6 kPa; F108-S: 15.13 ± 1.3 kPa) than control alginate scaffolds (REF-S: 27.13 ± 1.43 kPa). Control alginate scaffolds and Mx80-S presented a stable elastic modulus over the successive compressions, which suggested an elastic behavior. On the contrary, elastic moduli of Mx20-S, F127-S and F108-S were time-dependent and their mechanical behaviors in compression suggested viscous and/or plastic phenomena.

3.6. MSC seeding, viability and metabolic activity within 3D scaffolds

For *in vitro* experiments 20,000 human MSCs were seeded by centrifugation on each type of scaffold. Fig. 7A shows the distribution of cells through the thickness of the F108-S just after seeding (4 h). As suggested by the Live/Dead® labeling, cells were alive and were able to be seeded through the thickness of the scaffolds. Cell labeling and confocal microscopy observations were similar for all the examined scaffold types, which validates the cell seeding procedure.

Then we investigated cell metabolic activity after 3 and 14 days of culture within the porous scaffolds using Alamar Blue Assay. Fig. 7B shows the relative fluorescence intensity measured in the supernatant of the cell-seeded scaffolds. The results were normalized by the fluorescence intensity measured for 20,000 MSCs (the initial metabolic activity at the moment of seeding).

After 3 days of culture, a decrease in cell metabolic activity was observed in all types of scaffolds suggesting an early cell death or a decrease in metabolic activity. However, 14 days after seeding, the relative fluorescence intensity in all scaffolds has increased compared to that measured for MSCs on the day of seeding, indicating that all formulations supported long-term cell proliferation and/or increase in metabolic activity.

3.7. Secretion of paracrine factors by scaffold-seeded MSCs

Paracrine factors secreted by MSCs play a major role in beneficial effects of cell therapy. Previous studies showed that HGF, FGF-2 and VEGF may play an important role in mediating the beneficial effects of the MSCs in cell therapy of ischemic diseases (Efthimiadou et al., 2006; Gnecchi et al., 2008; Kitta et al., 2003; Mias et al., 2008, 2009; Rayssac et al., 2009; Tögel et al., 2007; Xin et al., 2001). Therefore, the functionality of MSCs was investigated by the quantification of HGF, FGF-2 and VEGF released in the supernatant of MSCs cultured in alginate macroporous scaffolds. Analyses were performed 24 h after cell seeding and the results were compared to the secretion level obtained from MSCs in a culture plate.

As shown in Fig. 8, we found that the secretion of HGF, FGF-2 and VEGF by the MSCs differed according to the scaffold type and culture conditions. Cells had a tendency to down-regulate HGF and VEGF secretions and to up-regulate FGF-2 secretion when cultivated in 3D conditions compared to 2D culture in a culture plate. Excepted for Mx80-S, the secretion profiles of the entrapped MSCs within scaffolds prepared using surfactant seemed to be improved in comparison with REF-S. This trend was particularly marked for HGF secretion within Mx20-S and F127-S

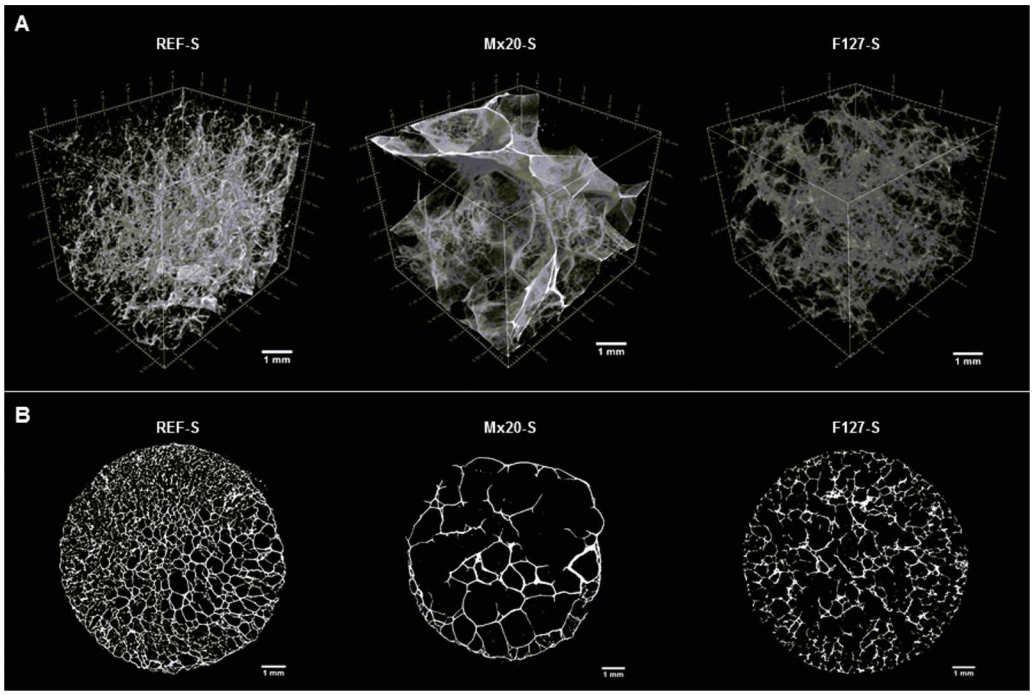

Fig. 3. Micro-CT analysis of scaffolds. (A) 3D micro-CT reconstruction of a ROI of REF-S, Mx20-S and F127-S. (B) 2D micro-CT images of the cross-section of the same scaffolds. The scale bar is 1 mm for both panels (A and B).

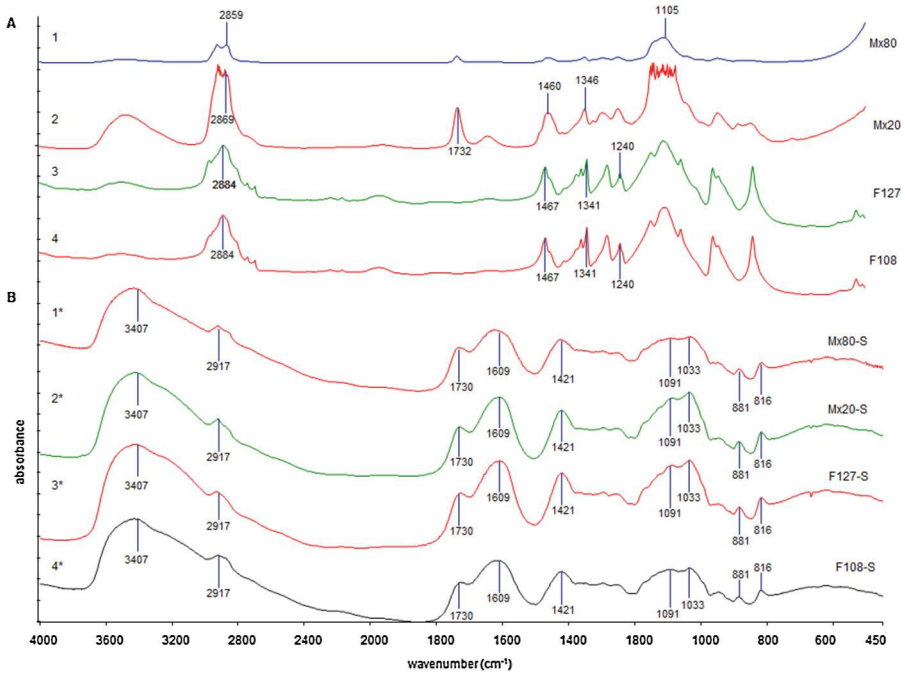

Fig. 4. FTIR analysis. (A) FTIR spectra and characteristic infrared peaks of surfactants: Mx80 (1), Mx20 (2), F127 (3) and F108 (4). (B) Final scaffolds FTIR spectra and characteristic peaks: Mx80-S (1*), Mx20-S (2*), F127-S (3*), and F108-S (4*).

(1.81 ± 1.28 pg/ml within Mx20-S and 1.47 ± 0.69 pg/ml within F127-S, $p > 0.05$ *vs* 0.22 ± 0.05 within REF-S) and became significant for VEGF secretion (19.31 ± 3.5 pg/ml within Mx20-S and 44.5 ± 13.04 pg/ml within F127-S, $p < 0.001$ *vs* 2.58 ± 0.5 within REF-S).

4. Discussion

Generating high porosity in implantable scaffolds is becoming a priority in tissue engineering and cell therapy. Indeed, an interconnected porosity has been reported to be indispensable for promoting good nutriment circulation, entrapped cell

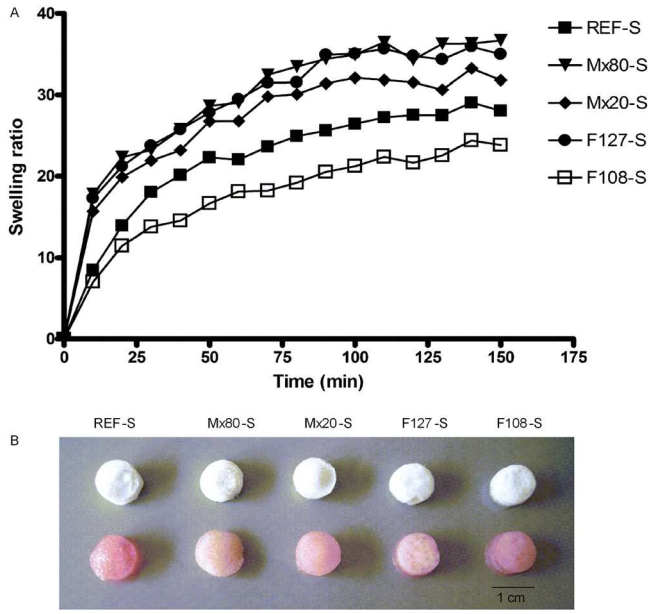

Fig. 5. Swelling behavior. (A) Swelling ratios of Mx80-S, Mx20-S, F127-S and F108-S as a function of sample immersion time in cell culture medium. (B) Scaffolds morphologies after rehydration in cell culture medium.

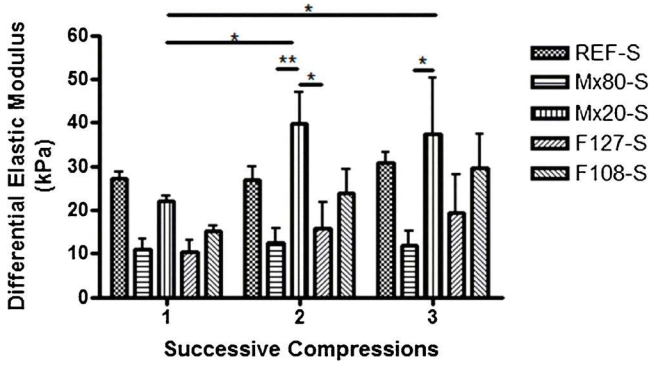

Fig. 6. Mechanical properties of macroporous scaffolds. Determination of the differential elastic moduli of macroporous scaffolds obtained under 3 successive compressions (1, 2 and 3) at 50% of strain. *: $p \leq 0.05$; **: $p \leq 0.01$, based on two-way Anova analysis.

migration and proliferation as well as for improving the long-term efficacy of the implanted device by favoring tissue integration and neovascularization. A consensus has been established on the necessity to generate an interconnected porous structure with pore size ranging from 50 to 300 μm (Mikos et al., 1993; Pittenger and Martin, 2004). However, this range needs to be adapted to the type of the delivered cells, to the targeted organ and to the treated pathology.

Different strategies have been described in the literature to obtain porosity in alginate scaffolds, particularly by utilizing different freezing regimes (Zmora et al., 2002), adding porogens (Hwang et al., 2010) or using foaming techniques (Eiselt et al., 2000; Barbetta et al., 2010; Andersen et al., 2012; Sharma et al., 2012; Bueno et al., 2014). Tailoring the porous architecture of 3D alginate scaffolds by changing the freezing regime holds the advantage of being a simple method however it does not allow fine control over porosity parameters (Zmora et al., 2002). In contrast, adding porogens (Hwang et al., 2010; Sergeeva et al., 2015) and/or using foaming techniques (Andersen et al., 2012; Barbetta et al., 2010; Bueno et al., 2014; Eiselt et al., 2000; Sharma et al., 2012) enable tuning additional operational parameters over hydrogels' porosity. The latter technique appears promising in providing highly macroporous 3D scaffolds but its real potential is yet to be explored as the final scaffold's biocompatibility and architecture may be greatly affected by foam composition, foam stability and operating conditions. The influence of parameters related to alginate macromolecular properties (Barbetta et al., 2010; Andersen et al., 2012, 2014a), gelling time, concentration and/or source of gelling ions (Andersen et al., 2012) as well as to surfactant concentration (Bueno et al., 2014; Eiselt et al., 2000) have been extensively studied. However, the influence of surfactant type on scaffold's characteristics has never been explored. Moreover, although globally dedicated to cell culture (Andersen et al., 2014b; Costantini et al., 2016), none of the previously described foam-based scaffolds have been designed for MSC culture to match the specific requirements of a given targeted organ and/or of a given cell source. The present paper is the first one to report a comparative study of alginate foam-based scaffolds for soft tissue engineering using MSCs. To that aim, we compared alginate matrices with various porosities and mechanical properties (produced using various surfactants), and shown that the scaffolds' architecture and performance can be controlled by the type of surfactant used.

Some protocols proposed in the literature avoid using surfactants because of their possible toxicity; however, the obtained porosity within the scaffold may be difficult to control in a reproducible manner. Consequently, an improvement of mechanical properties involving the use of a potentially toxic cross-linker (Sharma et al., 2012) may be required. In our study, we selected non-ionic highly hydrophilic surfactants, commonly used in biomedical applications (Andersen et al., 2012; Bueno et al., 2014; Eiselt et al., 2000; Fowler et al., 2002; Inzana et al., 2014; Tadros, 2005; Vashi et al., 2008), and washed them following the preparation step to preserve the final scaffolds' biocompatibility. Surfactant addition to alginate solutions appears to be an effective strategy for stabilizing the foam and, consequently, acquiring a homogenous porous structure after cross-linking. The use of these surfactants enabled obtaining stable foams, for the studied period of 120 min, thus permitting the preparation of foam-based scaffolds with largely homogeneous porosity in all structures.

Our scaffolds, prepared using several surfactants, differed with regard to their surface and cross-section porosity profiles. Therefore, scaffolds' microarchitectures can be controlled by varying the surfactant type. Also, for all scaffold types, surface porosity and pore interconnectivity allowed MSC seeding by centrifugation.

Mechanical resistance is another critical parameter affecting the final device's engraftment ability and its *in vivo* fate. In a previous study our group has determined, *in vitro* and *in vivo*, the influence of alginate type on 3D alginate scaffolds biocompatibility. We have shown that G-type alginate can improve mechanical properties of hydrogels without affecting MSC secretion capacity (Ceccaldi et al., 2012). Based on these results, we have chosen ultrapure G-type alginate and a high polymer concentration (3% w/w) in order to optimize the porous structures' mechanical properties. Measurements of the differential elastic moduli showed a slight loss of mechanical properties, but not significant, when porosity was generated in foam scaffolds (11–22 kPa) in comparison to control alginate scaffolds (27 kPa). This range of mechanical resistance matches soft tissues presenting elastic moduli between 1 and 20 kPa, depending on the considered organ (Engler et al., 2006).

Scaffolds' FTIR spectra did not show any trace of surfactant and their porosity supported MSC viability. The latter was maintained during 14 days, thus showing good *in vitro* biocompatibility of all alginate foam scaffolds. Furthermore, we observed that the seeded

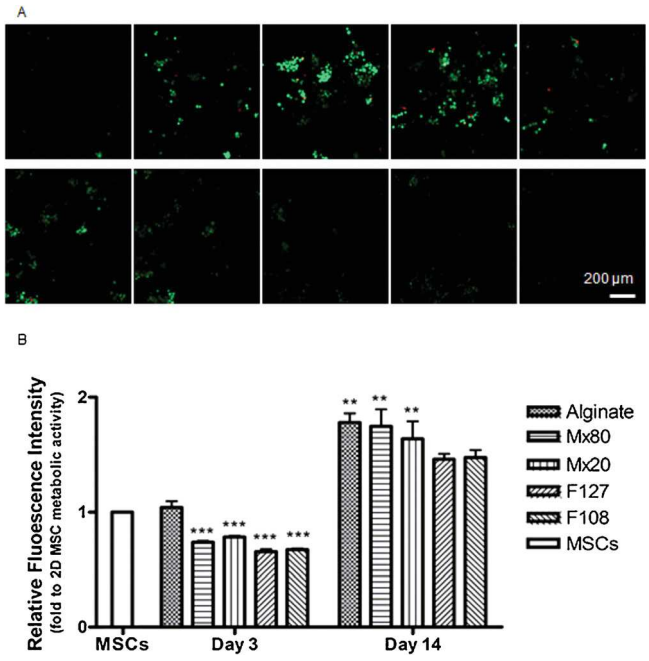

Fig. 7. Cell seeding and metabolic activity of human MSCs cultured within alginate macroporous scaffolds. (A) Confocal *z*-planes (from the surface: 1 to the bottom: 10) of MSC-seeded F108-S and a Live/Dead staining (live cells in green and dead cells in red) 4 h after seeding. Scale bar corresponds to 200 µm (magnification at 10×). (B) Alamar Blue assays performed 3 and 14 days after cell seeding. Results are fold to the fluorescence measured for 20,000 human MSCs in a culture plate (presented as MSCs in the figure). * denotes a significant difference compared to human MSCs on a culture plate (**: $p \leq 0.01$, ***: $p \leq 0.001$, based on Anova analysis). (For interpretation of the references to color in this figure legend, the reader is referred to the web version of this article.)

cells were retained within all of the tested scaffolds. This indicates that despite the non-cell adhesive nature of the alginate polymer, alginate porous scaffolds could constitute an excellent support for MSC delivery in cell therapy as they favor both cell survival and retention. *In vitro* results of the secretion levels obtained from MSCs revealed that growth factors release differed considerably depending on the conditions of culture and scaffold type. We found that when MSCs were grown within the scaffolds the secretion of FGF-2 increased and that the secretion of HFG and VEGF decreased, in comparison to cells grown in a culture plate. When comparing MSCs' secretory profiles within macroporous scaffolds, we found that they globally improved more when a surfactant was used in the preparation step than within control alginate scaffolds. Interestingly, for the three studied growth factors, cell secretion globally leveled-up more within Mx20-S and F127-S than within REF-S. These growth factors are well known to be involved in the positive effects of MSCs on tissue regeneration, particularly after an ischemic injury. Indeed, HGF is known to reduce the fibrotic response and to promote both cytoprotection and angiogenesis (Esposito et al., 2003; Jayasankar et al., 2005; Tomita et al., 2003; Wang et al., 2004). FGF-2 and VEGF are also widely described as being involved in blood vessels formation (Kim et al., 2011; Presta et al., 2005; Simons, 2004; Vandervelde et al., 2005). Since the functionality of the entrapped MSCs was best preserved within Mx20-S and F127-S, these formulations appear as most promising for regenerative engineering applications.

Given that surfactants generated various porous architectures and had different impacts on MSCs' paracrine activity, we further examined the porous structure of the different formulations by reconstructing a representative volume of each of them using micro-CT. The pore sizes of all scaffolds remained within the compatible range for 3D cell culture (50–300 µm) but notable differences existed in their pore density. Even though MSC metabolic activity was similar in all scaffold types, Mx20-S and F127-S presented lower pore densities than control scaffolds, both on surface and in cross-section. Furthermore, it was within Mx20-S and F127-S that cell secretion of growth factors was better preserved. Although the mechanisms responsible for the MSCs' paracrine activity changes in scaffolds are unclear, we can speculate that it could be related to the matrix 3D environment. Indeed, numerous researchers have reported that the scaffold's porosity could affect the cells' morphology, secretory functions and fate (Coutu et al., 2009; Dado and Levenberg, 2009; El-Ayoubi et al., 2008; Zehbe et al., 2010). Even though all authors agree that a highly porous and interconnected structure is necessary for the optimal diffusion of nutrients, gases and waste, the mechanisms responsible for the changes in cell characteristics and properties are not fully elucidated and there is no current consensus regarding the scaffold's optimal pore size for a given physiological process. A recent study comparing two- and three-dimensional culture conditions has shown that the latter enhanced the MSCs' paracrine immunomodulatory potential (Follin et al., 2016). Nevertheless, such an effect strongly varies with the scaffold's morphology and this particularity makes possible the design of tunable biomaterials adapted to specific application.

5. Conclusion

Our work presents for the first time a comparative study of various surfactants in association with alginate to generate highly porous scaffolds matching specifications required for MSC therapy. We used various foam stabilizing agents and compared their influence on matrix porosity, mechanical properties and secretion capacity of human MSCs. The range of their differential elastic

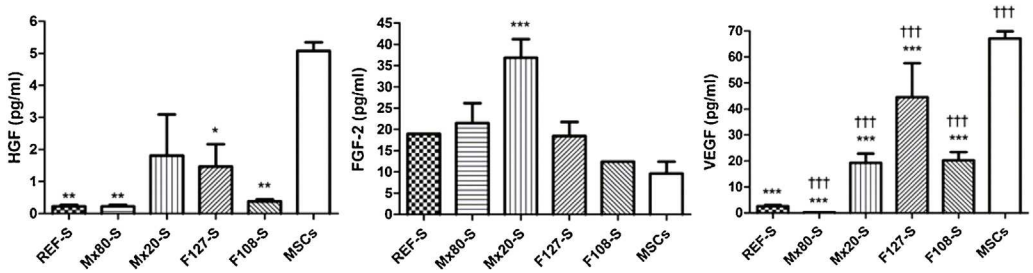

Fig. 8. Paracrine activity of seeded human MSCs. Quantification of HGF, FGF-2 and VEGF released in the supernatant by human MSCs cultured within macroporous scaffolds or in a culture Plate 24 h post-seeding. * denotes a significant difference compared to human MSCs in a culture plate (*: $p \leq 0.05$; **: $p \leq 0.01$, ***: $p \leq 0.001$, based on Anova analysis) and † denotes a significant difference compared human MSCs cultured within REF-S (†††: $p \leq 0.001$, based on Anova analysis).

moduli corresponds to that of soft tissues and their porosity can support cell proliferation and secretion of paracrine factors. These results suggest that the use of foams for the preparation of alginate scaffolds may improve the efficacy of MSCs in cell therapy, as an appropriate support for cell preservation during implantation. The *in vitro* evaluation of their compatibility with MSC viability, metabolic activity and secretion function supports the potential of this approach for cell therapy of soft tissues.

Author disclosure statement

No competing financial interests exist.

Acknowledgements

This work was supported by CNRS (CNRS grant for exploratory projects "Interface Matériau/Vivant"), INSERM and Région Midi-Pyrénées grants. We wish to thank the Cellular Imaging Facility (T. R.I. Genotoul Plateform, Toulouse, France).

References

Alfarano, C., Roubeix, C., Chaaya, R., Ceccaldi, C., Calise, D., Mias, C., Cussac, D., Bascands, J.L., Parini, A., 2012. Intraparenchymal injection of bone marrow mesenchymal stem cells reduces kidney fibrosis after ischemia-reperfusion in cyclosporine-immunosuppressed rats. Cell Transplant. 21, 2009–2019.

Andersen, T., Melvik, J.E., Gaserod, O., Alsberg, E., Christensen, B.E., 2012. Ionically gelled alginate foams: physical properties controlled by operational and macromolecular parameters. Biomacromolecules 13, 3703–3710.

Andersen, T., Melvik, J.E., Gaserod, O., Alsberg, E., Christensen, B.E., 2014a. Ionically gelled alginate foams: physical properties controlled by type, amount and source of gelling ions. Carbohydr. Polym. 99, 249–256.

Andersen, T., Markussen, C., Dornish, M., Heier-Baardson, H., Melvik, J.E., Alsberg, E., Christensen, B.E., 2014b. In situ gelation for cell immobilization and culture in alginate foam scaffolds. Tissue Eng. Part A 20, 600–610.

Andersen, T., Auk-Emblem, P., Dornish, M., 2015. 3D cell culture in alginate hydrogels. Microarrays (Basel) 4, 133–161.

Augst, A.D., Kong, H.J., Mooney, D.J., 2006. Alginate hydrogels as biomaterials. Macromol. Biosci. 6, 623–633.

Bajpai, S.K., Sharma, S., 2004. Investigation of swelling/degradation behaviour of alginate beads crosslinked with Ca^{2+} and Ba^{2+} ions. React. Funct. Polym. 59, 129–140.

Barbetta, A., Carrino, A., Costantini, M., Dentini, M., 2010. Polysaccharide based scaffolds obtained by freezing the external phase of gas-in-liquid foams. Soft Matter 6, 5213–5224.

Bidarra, S.J., Barrias, C.C., Granja, P.L., 2014. Injectable alginate hydrogels for cell delivery in tissue engineering. Acta Biomater. 10, 1646–1662.

Bueno, C.Z., Dias, A.M., de Sousa, H.J., Braga, M.E., Moraes, A.M., 2014. Control of the properties of porous chitosan-alginate membranes through the addition of different proportions of Pluronic F68. Mater. Sci. Eng. C: Mater. Biol. Appl. 44, 117–125.

Caplan, A.I., 2007. Adult mesenchymal stem cells for tissue engineering versus regenerative medicine. J. Cell. Physiol. 213, 341–347.

Ceccaldi, C., Fullana, S.G., Alfarano, C., Lairez, O., Calise, D., Cussac, D., Parini, A., Sallerin, B., 2012. Alginate scaffolds for mesenchymal stem cell cardiac therapy: influence of alginate composition. Cell Transplant. 21, 1969–1984.

Chen, S., Chen, L., Wu, X., Lin, J., Fang, J., Chen, X., Wei, S., Xu, J., Gao, Q., Kang, M., 2012. Ischemia post conditioning and mesenchymal stem cells engraftment synergistically attenuate ischemia reperfusion-induced lung injury in rats. J. Surg. Res. 178, 81–91.

Costantini, M., Colosi, C., Mozetic, P., Jaroszewicz, J., Tosato, A., Rainer, A., Trombetta, M., Święszkowski, W., Dentini, M., Barbetta, A., 2016. Correlation between porous texture and cell seeding efficiency of gas foaming and microfluidic foaming scaffolds. Mater. Sci. Eng. C: Mater. Biol. Appl. 62, 668–677.

Coutu, D.L., Yousefi, A.M., Galipeau, J., 2009. Three-dimensional porous scaffolds at the crossroads of tissue engineering and cell-based gene therapy. J. Cell. Biochem. 108, 537–546.

Dado, D., Levenberg, S., 2009. Cell-scaffold mechanical interplay within engineered tissue. Semin. Cell Dev. Biol. 20, 656–664.

Dvir, T., Kedem, A., Ruvinov, E., Levy, O., Freeman, I., Landa, N., Holbova, R., Feinberg, M.S., Dror, S., Etzion, Y., Leor, J., Cohen, S., 2009. Prevascularization of cardiac patch on the omentum improves its therapeutic outcome. Proc. Natl. Acad. Sci. U. S. A. 106, 14990–14995.

Dvir-Ginzberg, M., Elkayam, T., Cohen, S., 2008. Induced differentiation and maturation of newborn liver cells into functional hepatic tissue in macroporous alginate scaffolds. FASEB J. 22, 1440–1449.

Efthimiadou, A., Lambropoulou, M., Pagonopoulou, O., Vakalopoulos, I., Papadopoulos, N., Nikolettos, N., 2006. The role of basic-fibroblast growth factor (b-FGF) in cyclosporine-induced nephrotoxicity. In Vivo 20, 265–269.

Eiselt, P., Yeh, J., Latvala, R.K., Shea, L.D., Mooney, D.J., 2000. Porous carriers for biomedical applications based on alginate hydrogels. Biomaterials 21, 1921–1927.

El-Ayoubi, R., Eliopoulos, N., Diraddo, R., Galipeau, J., Yousefi, A.M., 2008. Design and fabrication of 3D porous scaffolds to facilitate cell-based gene therapy. Tissue Eng. Part A 14, 1037–1348.

Engler, A.J., Sen, S., Sweeney, H.L., Discher, D.E., 2006. Matrix elasticity directs stem cell lineage specification. Cell 126, 677–689.

Esposito, C., Parilla, B., De Mauri, A., Cornacchia, F., Fasoli, G., Foschi, A., Mazzullo, T., Plati, A.R., Scudellaro, R., Dal Canton, A., 2003. Hepatocyte growth factor (HGF) reduces the expression of profibrotic factors in human isolated glomeruli. Giorn. Ital. Nefrol. Organ Oufficiale Soc. Taliana Nefrol. 20, 376–380.

Follin, B., Juhl, M., Cohen, S., Perdersen, A.E., Kastrup, J., Ekblond, A., 2016. Increased paracrine immunomodulatory potential of mesenchymal stromal cells in three-dimensional culture. Tissue Eng. Part B Rev. 22, 322–329.

Fowler, E.B., Cuenin, M.F., Hokett, S.D., Peacock, M.E., McPherson III, J.C., Dirksen, T. R., Sharawy, M., Billman, M.A., 2002. Evaluation of pluronic polyols as carriers for grafting materials: study in rat calvaria defects. J. Periodontol. 73, 191–197.

Furuichi, K., Shintani, H., Sakai, Y., Ochiya, T., Matsushima, K., Kaneko, S., Wada, T., 2012. Effects of adipose-derived mesenchymal cells on ischemia-reperfusion injury in kidney. Clin. Exp. Nephrol. 16, 679–689.

Gandhi, J.K., Opara, E.C., Brey, E.M., 2013. Alginate-based strategies for therapeutic vascularization. Ther. Deliv. 4, 327–341.

Giovagnoli, S., Luca, G., Blasi, P., Mancuso, F., Schoubben, A., Arato, I., Calvitti, M., Falabella, G., Basta, G., Bodo, M., Calafiore, R., Ricci, M., 2015. Alginates in pharmaceutics and biomedicine: is the future so bright? Curr. Pharm. Des. 21, 4917–4935.

Glicklis, R., Shapiro, L., Agbaria, R., Merchuk, J.C., Cohen, S., 2000. Hepatocyte behavior within three-dimensional porous alginate scaffolds. Biotechnol. Bioeng. 67, 344–353.

Gnecchi, M., Zhang, Z., Ni, A., Dzau, V.J., 2008. Paracrine mechanisms in adult stem cell signaling and therapy. Circ. Res. 103, 1204–1219.

Grant, G.T., Morris, E.R., Rees, D.A., Smith, P.J.C., Thom, D., 1973. Biological interactions between polysaccharides and divalent cations – egg-box model. FEBS Lett. 32, 195–198.

Hwang, C.M., Sant, S., Masaeli, M., Kachouie, N.N., Zamanian, B., Lee, S.H., Khademhosseini, A., 2010. Fabrication of three-dimensional porous cell-laden hydrogel for tissue engineering. Biofabrication 2, 035003.

Inzana, J.A., Olvera, D., Fuller, S.M., Kelly, J.P., Graeve, O.A., Schwarz, E.M., Kates, S.L., Awad, H.A., 2014. 3D printing of composite calcium phosphate and collagen scaffolds for bone regeneration. Biomaterials 35, 4026–4034.

Jayasankar, V., Woo, Y.J., Pirolli, T.J., Bish, L.T., Berry, M.F., Burdick, J., Gardner, T.J., Sweeney, H.L., 2005. Induction of angiogenesis and inhibition of apoptosis by hepatocyte growth factor effectively treats postischemic heart failure. J. Card. Surg. 20, 93–101.

Kim, S.H., Moon, H.H., Kim, H.A., Hwang, K.C., Lee, M., Choi, D., 2011. Hypoxia-inducible vascular endothelial growth factor-engineered mesenchymal stem cells prevent myocardial ischemic injury. Mol. Ther. 19, 741–750.

Kitta, K., Day, R.M., Kim, Y., Torregroza, I., Evans, T., Suzuki, Y.J., 2003. Hepatocyte growth factor induces GATA-4 phosphorylation and cell survival in cardiac muscle cells. J. Biol. Chem. 278, 4705–4712.

Klock, G., Pfeffermann, A., Ryser, C., Grohn, P., Kuttler, B., Hahn, H.J., Zimmermann, U., 1997. Biocompatibility of mannuronic acid-rich alginates. Biomaterials 18, 707–713.

Lee, K.Y., Mooney, D.J., 2001. Hydrogels for tissue engineering. Chem. Rev. 101, 1869–1879.

Leinfelder, U., Brunnenmeier, F., Cramer, H., Schiller, J., Arnold, K., Vásquez, J.A., Zimmermann, U., 2003. A highly sensitive cell assay for validation of purification regimes of alginates. Biomaterials 24, 4161–4172.

Léobon, B., Roncalli, J., Joffre, C., Mazo, M., Boisson, M., Barreau, C., Calise, D., Arnaud, E., André, M., Pucéat, M., Pénicaud, L., Prosper, F., Planat-Bénard, V., Casteilla, L., 2009. Adipose-derived cardiomyogenic cells: in vitro expansion and functional improvement in a mouse model of myocardial infarction. Cardiovasc. Res. 83, 757–767.

Leor, J., Aboulafia-Etzion, S., Dar, A., Shapiro, L., Barbash, I.M., Battler, A., Granot, Y., Cohen, S., 2000. Bioengineered cardiac grafts: a new approach to repair the infarcted myocardium? Circulation 102 (19 Suppl. 3), III56–III61.

Li, M., Ikehara, S., 2013. Bone-marrow-derived mesenchymal stem cells for organ repair. Stem Cells Int. UNSP 132642.

Maurel, A., Azarnoush, K., Sabbah, L., Vignier, N., Le Lorc'h, M., Mandet, C., Bissery, A., Garcin, I., Carrion, C., Fiszman, M., Bruneval, P., Hagege, A., Carpentier, A., Vilquin, J.T., Menasché, P., 2005. Can cold or heat shock improve skeletal myoblast engraftment in infarcted myocardium? Transplantation 80, 660–665.

Mias, C., Trouche, E., Seguelas, M.H., Calcagno, F., Dignat-George, F., Sabatier, F., Piercecchi-Marti, M.D., Daniel, L., Bianchi, P., Calise, D., Bourin, P., Parini, A., Cussac, D., 2008. Ex vivo pretreatment with melatonin improves survival, proangiogenic/mitogenic activity, and efficiency of mesenchymal stem cells injected into ischemic kidney. Stem Cells 26, 1749–1757.

Mias, C., Lairez, O., Trouche, E., Roncalli, J., Calise, D., Seguelas, M.H., Ordener, C., Piercecchi-Marti, M.D., Auge, N., Salvayre, A.N., Bourin, P., Parini, A., Cussac, D., 2009. Mesenchymal stem cells promote matrix metalloproteinase secretion by cardiac fibroblasts and reduce cardiac ventricular fibrosis after myocardial infarction. Stem Cells 27, 2734–2743.

Mikos, A.G., Sarakinos, G., Lyman, M.D., Ingber, D.E., Vacanti, J.P., Langer, R., 1993. Prevascularization of porous biodegradable polymers. Biotechnol. Bioeng. 42, 716–723.

Panfilov, I.A., de Jong, R., Takashima, S., Duckers, H.J., 2013. Clinical study using adipose-derived mesenchymal-like stem cells in acute myocardial infarction and heart failure. Methods Mol. Biol. 1036, 207–212.
Pittenger, M.F., Martin, B.J., 2004. Mesenchymal stem cells and their potential as cardiac therapeutics. Circ. Res. 95, 9–20.
Presta, M., Dell'Era, P., Mitola, S., Moroni, E., Ronca, R., Rusnati, M., 2005. Fibroblast growth factor/fibroblast growth factor receptor system in angiogenesis. Cytokine Growth Factor Rev. 16, 159–178.
Rayssac, A., Neveu, C., Pucelle, M., Van den Berghe, L., Prado-Lourenco, L., Arnal, J.F., Chaufour, X., Prats, A.C., 2009. IRES-based vector coexpressing FGF2 and Cyr61 provides synergistic and safe therapeutics of lower limb ischemia. Mol. Ther. 17, 2010–2019.
Ruvinov, E., Cohen, S., 2016. Alginate biomaterial for the treatment of myocardial infarction: progress, translational strategies, and clinical outlook: from ocean algae to patient bedside. Adv. Drug Deliv. Rev. 96, 54–76.
Salem, A.K., Stevens, R., Pearson, R.G., Davies, M.C., Tendler, S.J., Roberts, C.J., Williams, P.M., Shakesheff, K.M., 2002. Interactions of 3T3 fibroblasts and endothelial cells with defined pore features. J. Biomed. Mater. Res. 61, 212–217.
Sapir, Y., Kryukov, O., Cohen, S., 2011. Integration of multiple cell–matrix interactions into alginate scaffolds for promoting cardiac tissue regeneration. Biomaterials 32, 1838–1847.
Sergeeva, A., Feoktistova, N., Prokopovic, V., Gorin, D., Volodkin, D., 2015. Design of porous alginate hydrogels by sacrificial $CaCO_3$ templates: pore formation mechanism. Adv. Mater. Interfaces 2, 1500386.
Shachar, M., Cohen, S., 2003. Cardiac tissue engineering, ex-vivo: design principles in biomaterials and bioreactors. Heart Fail. Rev. 8, 271–276.
Shapiro, L., Cohen, S., 1997. Novel alginate sponges for cell culture and transplantation. Biomaterials 18, 583–590.
Sharma, C., Dinda, A.K., Mishra, N.C., 2012. Fabrication and characterization of natural origin chitosan–gelatin–alginate composite scaffold by foaming method without using surfactant. J. Appl. Polym. Sci. 127, 3228–3241.
Silva, K.A., Juenet, M., Meddahi-Pellé, A., Letourneur, D., 2015. Polysaccharide-based strategies for heart tissue engineering. Carbohydr. Polym. 116, 267–277.
Simons, M., 2004. Integrative signaling in angiogenesis. Mol. Cell. Biochem. 264, 99–102.
Souidi, N., Stolk, M., Seifert, M., 2013. Ischemia-reperfusion injury: beneficial effects of mesenchymal stromal cells. Curr. Opin. Organ Transplant. 18, 34–43.
Tadros, T.F., 2005. Applied Surfactants: Principles and Applications, 1st ed. Wiley-VCH, Berkshire.
Tam, S.K., Dusseault, J., Polizu, S., Menard, M., Halle, J.P., Yahia, L., 2006. Impact of residual contamination on the biofunctional properties of purified alginates used for cell encapsulation. Biomaterials 27, 1296–1305.
Tögel, F., Weiss, K., Yang, Y., Hu, Z., Zhang, P., Westenfelder, C., 2007. Vasculotropic, paracrine actions of infused mesenchymal stem cells are important to the recovery from acute kidney injury. Am. J. Physiol. Renal Physiol. 292, F1626–F1635.
Toma, C., Pittenger, M.F., Cahill, K.S., Byrne, B.J., Kessler, P.D., 2002. Human mesenchymal stem cells differentiate to a cardiomyocyte phenotype in the adult murine heart. Circulation 105, 93–98.
Tomita, N., Morishita, R., Taniyama, Y., Koike, H., Aoki, M., Shimizu, H., Matsumoto, K., Nakamura, T., Kaneda, Y., Ogihara, T., 2003. Angiogenic property of hepatocyte growth factor is dependent on upregulation of essential transcription factor for angiogenesis, ets-1. Circulation 107, 1411–1417.
Trouche, E., Girod Fullana, S., Mias, C., Ceccaldi, C., Tortosa, F., Seguelas, M.H., Calise, D., Parini, A., Cussac, D., Sallerin, B., 2010. Evaluation of alginate microspheres for mesenchymal stem cell engraftment on solid organ. Cell Transplant. 19, 1623–1633.
Vandervelde, S., van Luyn, M.J., Tio, R.A., Harmsen, M.C., 2005. Signaling factors in stem cell-mediated repair of infarcted myocardium. J. Mol. Cell. Cardiol. 39, 363–376.
Vashi, A.V., Keramidaris, E., Abberton, K.M., Morrison, W.A., Wilson, J.L., O'Connor, A. J., Cooper-White, J.J., Thompson, E.W., 2008. Adipose differentiation of bone marrow-derived mesenchymal stem cells using Pluronic F-127 hydrogel in vitro. Biomaterials 29, 573–579.
Wang, Y., Ahmad, N., Wani, M.A., Ashraf, M., 2004. Hepatocyte growth factor prevents ventricular remodeling and dysfunction in mice via Akt pathway and angiogenesis. J. Mol. Cell. Cardiol. 37, 1041–1052.
Xin, X., Yang, S., Ingle, G., Zlot, C., Rangell, L., Kowalski, J., Schwall, R., Ferrara, N., Gerritsen, M.E., 2001. Hepatocyte growth factor enhances vascular endothelial growth factor-induced angiogenesis in vitro and in vivo. Am. J. Pathol. 158, 1111–1120.
Yip, H.K., Chang, Y.C., Wallace, C.G., Chang, L.T., Tsai, T.H., Chen, Y.L., Chang, H.W., Leu, S., Zhen, Y.Y., Tsai, C.Y., Yeh, K.H., Sun, C.K., Yen, C.H., 2013. Melatonin treatment improves adipose-derived mesenchymal stem cell therapy for acute lung ischemia-reperfusion injury. J. Pineal Res. 54, 207–221.
Zehbe, R., Goebbels, J., Ibold, Y., Gross, U., Schubert, H., 2010. Three-dimensional visualization of in vitro cultivated chondrocytes inside porous gelatine scaffolds: a tomographic approach. Acta Biomater. 6, 2097–2107.
Zeltinger, J., Sherwood, J.K., Graham, D.A., Mueller, R., Griffith, L.G., 2001. Effect of pore size and void fraction on cellular adhesion, proliferation, and matrix deposition. Tissue Eng. 7, 557–572.
Zieber, L., Or, S., Ruvinov, E., Cohen, S., 2014. Microfabrication of channel arrays promotes vessel-like network formation in cardiac cell construct and vascularization in vivo. Biofabrication 6, 024102.
Zmora, S., Glicklis, R., Cohen, S., 2002. Tailoring the pore architecture in 3-D alginate scaffolds by controlling the freezing regime during fabrication. Biomaterials 23, 4087–4094.